Influence of fiber content on C/C-SiC brake materials fabricated by compression molding and hot sintering

Chen Tang*, Alei Dang, Tiehu Li, Tingkai Zhao, Hao Li, Shasha Jiao

State Key Laboratory of Solidification Processing, School of Materials Science and Engineering, Northwestern Polytechnical University, Xi'an, 710072, PR China

ARTICLE INFO

ABSTRACT

In this work, short carbon fibers were utilized as reinforcing materials to incorporate with C-SiC ceramics. C_f/C-SiC composites containing diverse fiber contents were fabricated by combining compression molding and hot sintering. Mechanical and tribological properties were carefully investigated. The result indicates that 30 vol% fiber content composite shows the highest flexural strength (201.42 MPa) and shear strength (116.68 MPa). The reinforcing mechanisms are summarized as fiber pulling-out, fiber debonding and fiber bridging, as well as crack deflection. Tribological testing reveals that 30% fiber content composite shows the strongest wear resistance (3.95×10^{-6} mm^3/N·m) and cyclic performances (COF of 0.27 after 50 cycles). The friction mechanisms are divided into abrasive wear, adhesion wear and oxidation wear by different wear stages.

1. Introduction

Carbon fiber reinforced carbon black and silicon carbide dual matrices composite (C_f/C-SiC) has been considered as the most promising brake material and received extensive attention in recent years [1–3]. This composite material not only inherits the excellent mechanical properties and tribological performances of traditional C/C materials, but also exhibits improved properties such as high thermal shock resistance, long service life, and high environmental stability, owing to the good thermodynamic performance of SiC matrix under high temperature [4,5]. These improved properties of C_f/C-SiC composite provide reliable evidence for its practical application in automobile brake systems, which have been successfully applied on Porsche 911, Benz AMG and Audi A8 [6]. Even in the military and aerospace fields, C_f/C-SiC composite still shows great prospects. Studies show that the friction efficiency of the C/C-SiC disc and pad brake system on a military tank is three times higher than that of metallic brake systems [7]. In 2008, C/C-SiC brake pairs were first applied to an airplane for a trial flight and achieved satisfactory results [8].

The main difficulty in fully exploring short carbon fiber reinforced composites lie in the apparent impediment to effectively model their geometry at micro-level [9]. Carbon fibers preforms, including 2D woven cloth and 3D felt, were widely utilized as reinforcing materials to incorporate with C-SiC dual matrices [10–12]. Although the obtained composite keeps most of the superior properties of the carbon fibers, it still inclines to delaminate under elevated shear forces due to the weak interfacial adhesion between different layers. Meanwhile, the porous structure of 3D carbon felt usually restricts the diffusion of ceramic matrices during vapor deposition. These shortcomings often lead to catastrophic failure in its practical application [13,14]. Compared with continuous carbon fibers, short carbon fibers provide larger specific contact area which facilitate the formation of interfacial phase between the fiber and the matrix. The obtained composite also shows high degree of isotropic due to the free orientations of short carbon fibers in matrix, their strength and toughness are improved as well [15–17].

Among several eminent endeavors [18–21], a short carbon fiber reinforced composite fabricated in Li's group [22] relished considerable support, the composite shows a significantly enhanced fracture toughness and flexural strength. After years of development, the coefficient of friction (COF) and stability of the composites have been highly improved by increasing fiber content and reducing porosity [23,24]. So far, most C_f/C-SiC composites were fabricated by hot pressing followed with sintering [25]. Prior to fabricate, it is necessary to introduce pretreatment process to modify carbon fiber surfaces, due to their poor wettability and high chemical inertness [26]. In addition, free silicon in the matrices are also found of great influence on creep resistance of the composites [27].

The present work focused on preparation and characterization of C_f/C-SiC composites with enhanced mechanical and tribological properties. Composites with diverse fiber content were fabricated by combining compression molding and hot sintering. Microstructures of the composites were carefully studied. The effect of fiber content on

---

* Corresponding author.
  E-mail address: mecdoll@yahoo.com (C. Tang).

flexural strength and shear strength was further explored. Their potentials as alternative braking materials to incorporate with SiC balls were also carefully investigated in dry conditions. The results reveal that fiber content indeed had great influence on friction behaviors of C_f/C-SiC composites, given the composites enormous potential to supersede traditional braking systems.

2. Experimental

2.1. Raw materials

PAN-based carbon fibers (T700, Toray, Japan) with a diameter of 7 μm were employed as reinforcing materials. Their tensile strength and elastic modulus are of 3500 MPa and 240 GPa, according to the information from the manufacturer. Ceramic powders like silicon (size of 30–50 μm, purity ≥ 99.8%) and carbon black (size of 6–8 μm, purity ≥ 99.9%) were utilized as substrate materials. Other starting solvents like ethyl alcohol (purity ≥ 99.7%), acetone (purity ≥ 98%) and nitric acid (concentration of 65–68%) were obtained from commercial vendors and used without further purification.

2.2. Preparation

Continuous PAN-based long carbon fibers were cut into short bundles of 5–8 mm by a paper cutter, then socked in acetone solution helped with ultrasonic vibration for 8 h to remove sediment and contaminant on fiber surfaces and ensure their uniform dispersion at random orientations. Afterwards, the randomly distributed short carbon fibers were immersed in 35% nitric acid solution for 4 h at 40 °C, for purpose of increasing specific surface area and attaching oxygen-containing functional groups such as hydroxyl (-OH), carbonyl (-C=O) and carboxyl (-COOH) [28–30]. The modified carbon fibers then were washed repeatedly with deionized water and dried in a vacuum oven for subsequent use [31,32].

In the mixing process, Si and C powders (in a ratio of 1:1.5) were ball milled in a planetary grinding machine for 1 h to ensure the uniform dispersion. Then, carbon fibers of different volume fraction (10, 20, 30, 40%) were mixed with the matrix materials using ethanol as the media and ball milled for 15 min. Since extensive grinding can damage the strength of carbon fiber, the milling time should be controlled in a reasonable range. Afterwards, the mixture was injected into an iron cast mold which was pre-heated at 150 °C in advance, then compressed at 20 MPa for 2 h. The obtained preforms were heated at 1600 °C for 1 h in an argon atmosphere to ensure the full conversion of silicon carbide from C and Si. The obtained composites were polished and cut into specific size of testing requirements.

2.3. Characterizations

Open porosity and bulk density were quantified by Archimedes' method. Composites were weighted by an electronic balance with a precision of 0.1 mg. Phase identification was examined by X-ray diffraction (XRD) using Cu K_α radiation (λ = 0.15405 nm) on a Rigaku D/Max-2400 diffractometer, by a scanning speed of 5°/min and scanning range of 10–90°. Microstructures and surface morphology were investigated by JSM-6700F field emission scanning electronic microscope (FE-SEM, ZEISS, Germany) equipped with energy dispersive spectroscopy (EDS).

Mechanical properties such as flexural strength and shear strength were verified on a standard electronic universal testing machine (CMT1505, INSTRON, American). Composites were cut into size of $50 \times 10 \times 4 \, mm^3$ for flexural testing, and $36 \times 10 \times 6 \, mm^3$ for shear testing. Both loading rate was set to 0.5 mm/min, with 40 mm and 24 mm span, respectively. Tribological properties of the composite mated with SiC ball (6 mm in diameter) were investigated on a UMT-2MT friction machine by ball-on-disk method, with parameter of 10 N
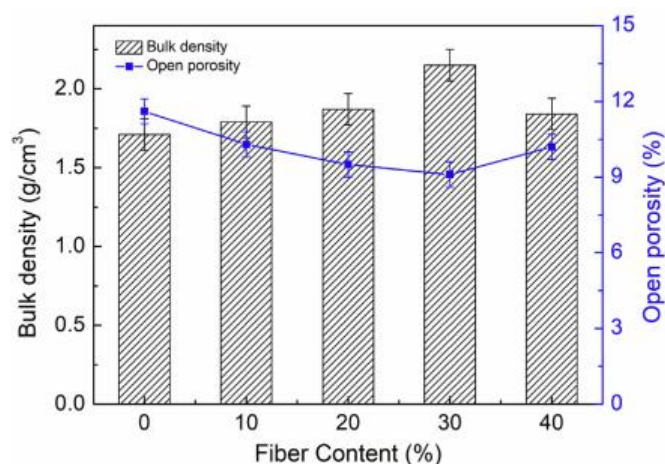
Fig. 1. Bulk density and open porosity of the C_f/C-SiC composites containing diverse carbon fiber content.

load at a speed of 180 r/min for 30 min under dry condition in air [18]. All samples were cleaned with ethanol and polished before testing.

3. Results and discussion

3.1. Microstructural analysis

Fig. 1 shows bulk density and open porosity of the composites with carbon fiber content rising from 0 to 40 vol%. It is observed that the bulk density varies from 1.71 to 2.15 g/cm³, while the open porosity fluctuates within the interval of 9.1–11.6%. During the sintering process, the matrix inclines to shrinkage, leaving large numbers of cracks and open pores within the composite. As the temperature reaches the glass transition point, the molten silicon spontaneously infiltrates into these vacancies under capillary force. However, as the fiber content exceeds 30%, the agglomeration of short carbon fibers prevents the impregnation process, thereby restricting further densification of the composite. In general, composite with 30 vol% fiber content shows the highest density (2.15 g/cm³) and lowest open porosity (9.1%).

XRD patterns of C_f/C-SiC composites containing diverse fiber content are depicted in Fig. 2. The formation of β-SiC (cubic phase) is observed in each XRD curve, which can be indexed as (111), (200), (220) and (311) planes of β-SiC at 2θ degrees of 35.59°, 41.38°, 59.97° and 71.77° (JCPDS No. 29–1129), respectively. Other diffraction peaks
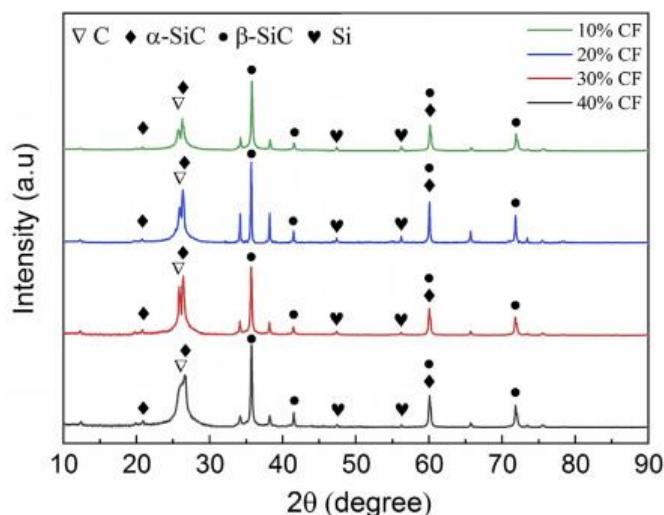
Fig. 2. XRD patterns of C_f/C-SiC composites containing diverse fiber content.
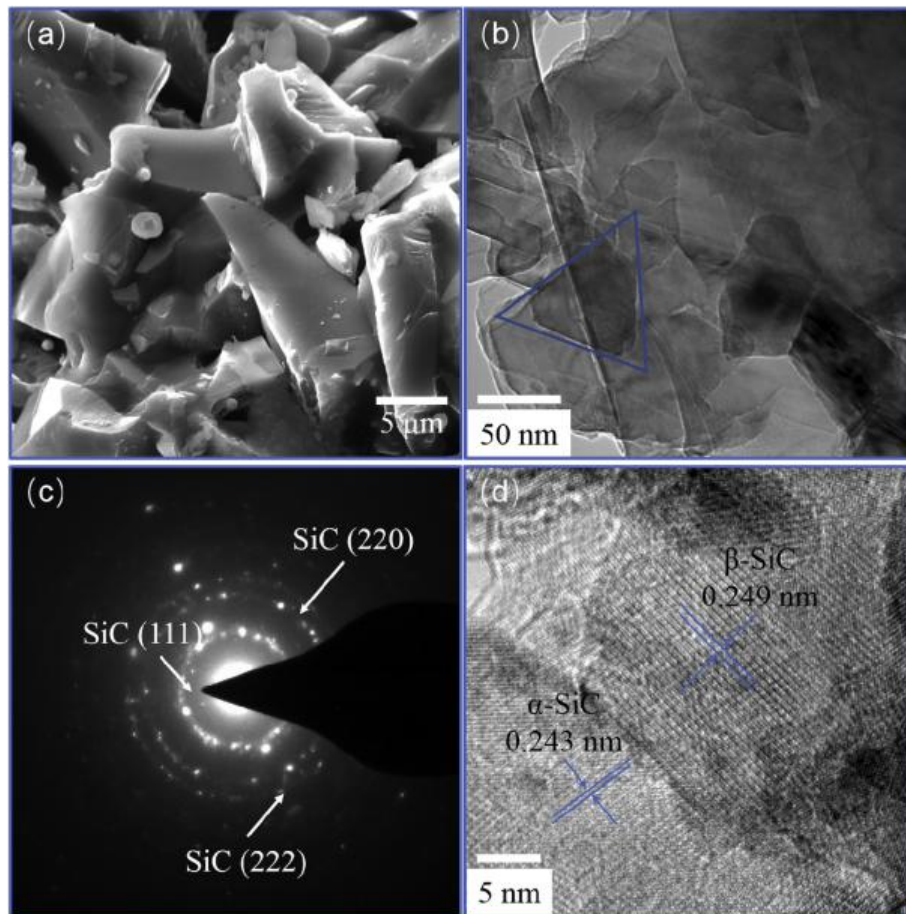
Fig. 3. SEM (a) and TEM (b, c, d) images of the SiC matrix.

at 2θ degree of 26.38°, 28.44°, 47.30° and 56.12° can be attributed to the characteristic planes of cubic Si (JCPDS No. 27–1402) and C in form of graphite (JCPDS No. 41–1487). Since the ratio of silicon to carbon in raw materials was 1–1.5, most of the silicon has converted into SiC, only a small amount of unreacted free silicon remains in the matrix, presenting weak-intensity diffraction peaks. Meanwhile, α-SiC (hexagonal phase) is also detected from its representative peaks at 20.85°, 26.63° and 50.13° (JCPDS No. 29–1127), indicating the phase transition from β→α had occurred during sintering at high temperature of 1600 °C, which is consistent with the work presented by Lodhe [33].

The XRD results are also confirmed by SEM and TEM analysis. In Fig. 3a, the matrices present porous surface morphology, with large numbers of cracks and open pores distributing in it. These micropores are ascribed to the volume shrinkage of SiC during fabrication, providing a good coincidence with the work presented by Lee [34], in where a porous SiC ceramic was formed by rapid grain growth after β→α transformation. Fig. 3c shows the corresponding SEAD patterns of the triangle area in Fig. 3b, which can be indexed to β-SiC, indicating the SiC phase had successfully synthesized from Si and C. The HRTEM image in Fig. 3d confirms two uniform interplanar spacing of 0.249 nm and 0.243 nm with complete crystal structures, which match very well with the (111) plane of β-SiC and (101) plane of α-SiC.

Fig. 4 show polished surfaces and microstructures of 30% fiber content C_f/C-SiC composites at different magnifications. In Fig. 4a and b, short strips of carbon fibers are found uniformly distributed in C-SiC matrices at random orientations. The continuous gray phase corresponds to the β-SiC while the isolate light phase belongs to the α-SiC phase, which further confirms the XRD and TEM results. The interface with larger magnification between the fiber and the matrix is shown in Fig. 4c, suggesting a strong interfacial adhesion. As the most potential

reinforcement of composite materials, carbon fiber has the advantages of high strength, high modulus and lightweight [5]. However, it is susceptible to erosion by molten silicon at elevated temperature. The diameter of the carbon fiber became significantly smaller in Fig. 4c, indicating carbon atoms on fiber surfaces have been consumed by free silicon. As shown in Fig. 4d, defects like pits and flaws are also observed on carbon fiber surfaces.

3.2. Mechanical testing

Unlike conventional metal and non-metal materials, the chemical bonds of C_f/C-SiC composites fabricated by our group can be divided into two categories: covalent bonds between the matrix molecules and ionic bonds between the fiber and the matrix. These differences resulting a quite different fracture mechanism of C_f/C-SiC composite than the "brittle deformation" of ceramics and "plastic deformation" of metallic materials. As shown in Fig. 5a, all flexural strength-strain curves climb slightly at beginning then fall sharply. Compared to ceramic materials, a slow decline appears on each curve of C_f/C-SiC as the load reaches the maximum, suggesting the significant strengthening effect of carbon fibers to matrix. When catastrophic failure happens, residual carbon fibers could still carry most internal stress and restrict the propagation of the cracks, which enable the composites to withstand larger deformation. It is observed that 30 vol% fiber content composite shows the highest flexural strength (201.42 MPa), while 40 vol% fiber composite shows decreased flexural strength, which is even lower than that in 20 vol%.

The shear strength-strain curves of the C_f/C-SiC composites containing diverse fiber content are shown in Fig. 5b. It is concluded that the effect of fiber content on shear strength depicts similar changing
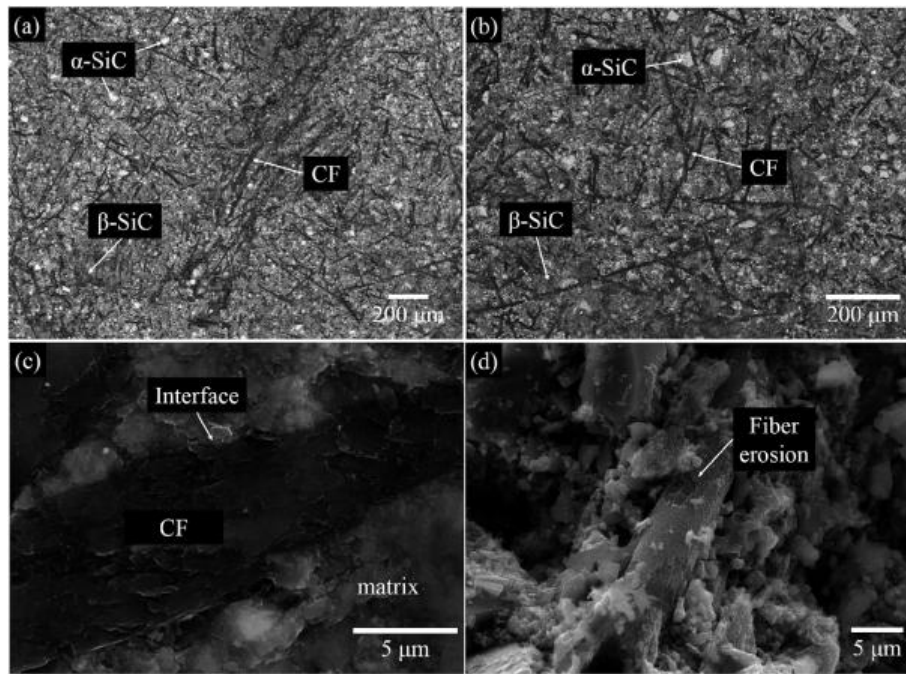
Fig. 4. Polished surfaces (a and b) and microstructures (c and d) of 30% fiber content C_f/C-SiC composites at larger magnifications.

trend than that on flexural strength. As the load reaching the maximum, each curve drops suddenly without slow decline. This can be attributed that during fabricating, the orientations of randomly distributed carbon fibers incline to be consistent (As shown in Fig. 4a and b, most carbon fibers in visual field are parallel to the principal plane). That means a layered structure is formed within the composite, and the energy required to delamination becomes much less than that needed for fiber breakage. Compared with the slow decline of flexural strength, the shear strength of the C_f/C-SiC composite drops significantly, with the highest value appearing at 116.68 MPa as the fiber content achieves 30 vol%. A comparative study of our work and the data provided by other researchers is shown in Table 1.

Fig. 6a–d presents the fracture surfaces of C_f/C-SiC composites containing diverse fiber content. Fiber pulling-out is observed in each case, which can be considered as the primary reinforcing mechanism in the fracture process. In Fig. 6a, only a small amount of carbon fiber was pulled-out from the matrix due to its low content (10%) in composite. This result changes as the fiber content increases, the improved specific contact area between the fiber and the matrix effectively transmit the internal stress and consumes more energy. As shown in Fig. 6b and c, a strong interfacial adhesion is observed between the fiber and the matrix, with a relatively flat fracture surface and short length of pulled-out

fibers. On the contrary, fiber agglomeration occurs at high fiber content to form poorly dispersed bundles (40% in Fig. 6d), resulting in an increased porosity and large numbers of microcracks. In Fig. 6e, the crack shows a jagged morphology which propagates along the load direction, the strong interfacial adhesion deflects the crack until they run through the entire composite. In addition, fiber debonding and fiber bridging are also found of great influence on mechanical properties of C_f/C-SiC, which can be clearly seen from the insert images in Fig. 6c and e.

3.3. Tribological testing

The effects of fiber content on COF and specific wear rate are presented in Fig. 7a. The COF of the composite containing 0% fiber content shows the highest average value of 0.47, then declines from 0.38 to 0.23 with the fiber content increasing from 10% to 40%. Compared to the SiC matrix, low carbon fiber content provides insufficient specific contact area on wear surface, thus resulting in lower COF of the composite due to the low COF of carbon fiber itself. On the other hand, the specific wear rate draws a quite different picture. The sharp decline starts from 10% fiber content composite, then reaches the minimum at an average rate of 3.95×10^{-6} mm³/N·m at 30%, followed with an uptrend to 40%. Reasonable explanation is that higher fiber content
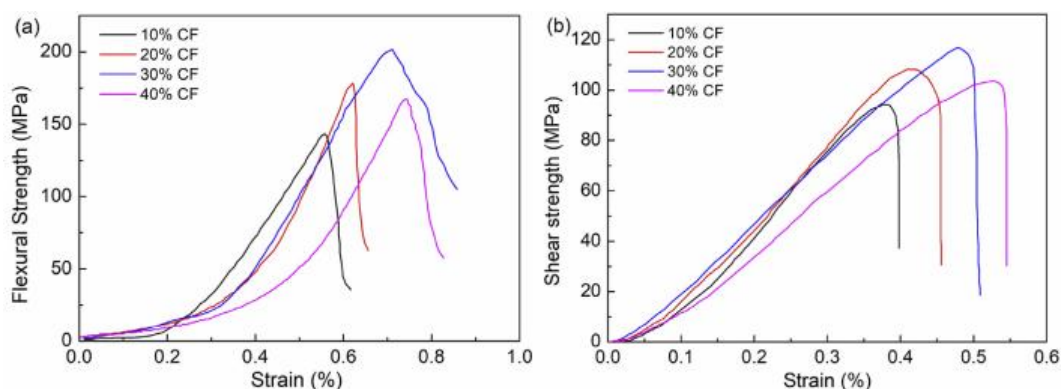
Fig. 5. Flexural (a) and shear (b) strength-strain curves of the C_f/C-SiC composites containing diverse fiber content.

Table 1
A comparative study of our work and data from other researchers.

Samples	Density (g/cm^3)	Porosity (%)	Flexural strength (MPa)	Shear strength (MPa)	Ref.
C/C-SiC (30% C$_f$)	2.15 ± 0.05	9.1 ± 0.5	201.42 ± 10	116.68 ± 10	Our work
C/C-HZS	2.23 ± 0.06	11.4 ± 0.3	172 ± 8	–	[35]
C/C-ZrC-ZrB$_2$-SiC	1.98	13.02	132	–	[36]
C/C-ZrC-SiC	1.66	16.86	187.2 ± 40.4	–	[37]

created large numbers of micropores or voids inside the composite, this porous structure is more likely to wear under higher pressure and shear force during the friction process, thereby increasing the specific wear rate.

Fig. 7b compares the COF curves of C$_f$/C-SiC composites containing 0% and 30% fiber content. At the prior stage of friction, both curves climb rapidly due to the increasing severe contact of the friction pairs. After reaching the maximum, both curves tend to be relatively smooth and fluctuate in a small range. This fluctuation can be attributed to the non-uniform wear track or the stick-slip mechanism [38,39]. Compared to the red curve, the black curve shows a larger average COF value which fluctuates in a larger range, providing reliable evidence to the results presented in Fig. 7a.

Since the 30% fiber content composites show the lowest COF and best wear resistance, they were chosen as the most promising brake materials to serve under cyclic conditions. Its wear mechanism is explained in detail combining the SEM analysis. In the prior stage of friction, the wear surface of the composite was almost flat with a small number of tiny asperities (Fig. 8a). As the friction pair violently coupled with each other, the tiny asperities were peeled off by the elevated shear force to generate debris on wear surface (Fig. 8b), which were turned out to be SiC particles by EDS analysis. Meanwhile, damaged carbon fibers were also observed on the wear surface and were subsequently ground to powders. These SiC debris and carbon powders became the abrasive medium for the next wear cycles by reducing the severe contact between the friction pairs. Considering the higher content and hardness of SiC debris than carbon powders, the wear mechanism at this stage was dominated by the abrasive wear of SiC debris which activated the "ploughing effect" to create scratches and grooves on wear surface (Fig. 8d) [40,41]. Studies also show that smaller crystal
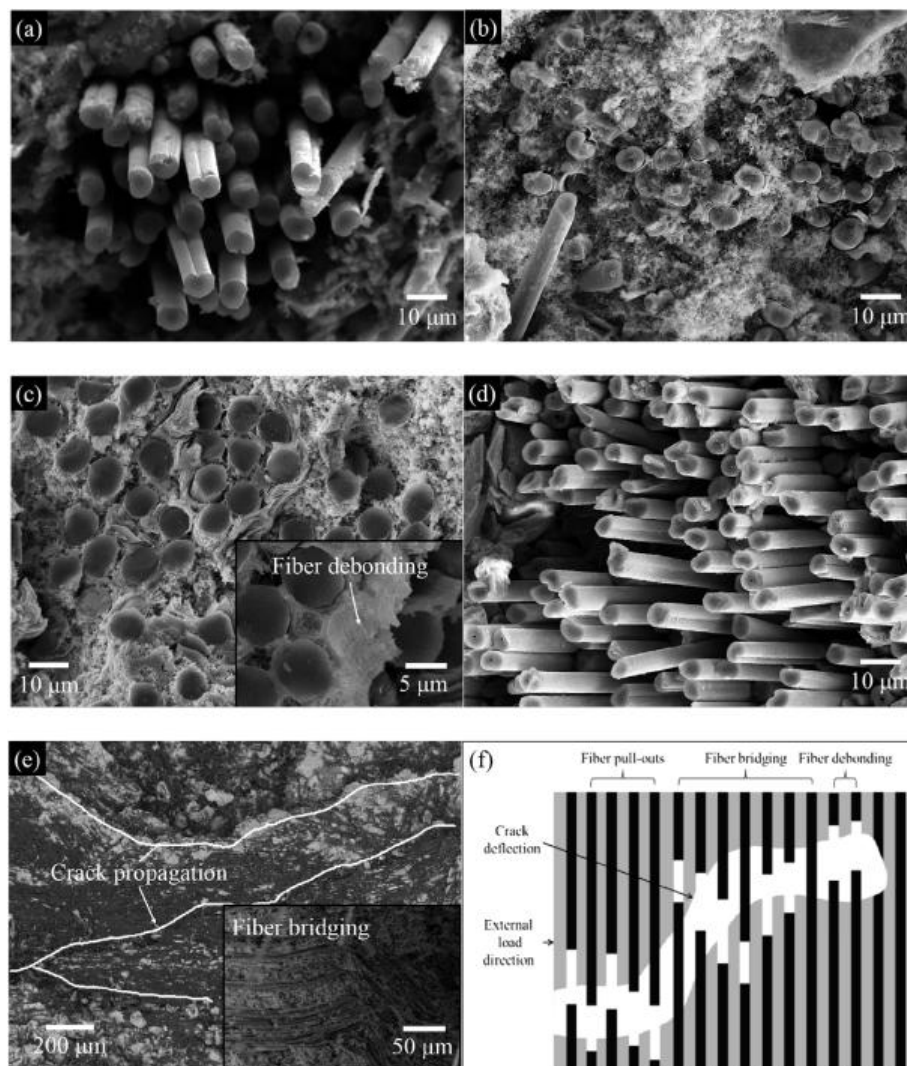
Fig. 6. Fracture surfaces of (a) 10%, (b) 20%, (c) 30% and (d) 40% C$_f$/C-SiC composite, (e) crack propagations and (f) fracture mechanism.
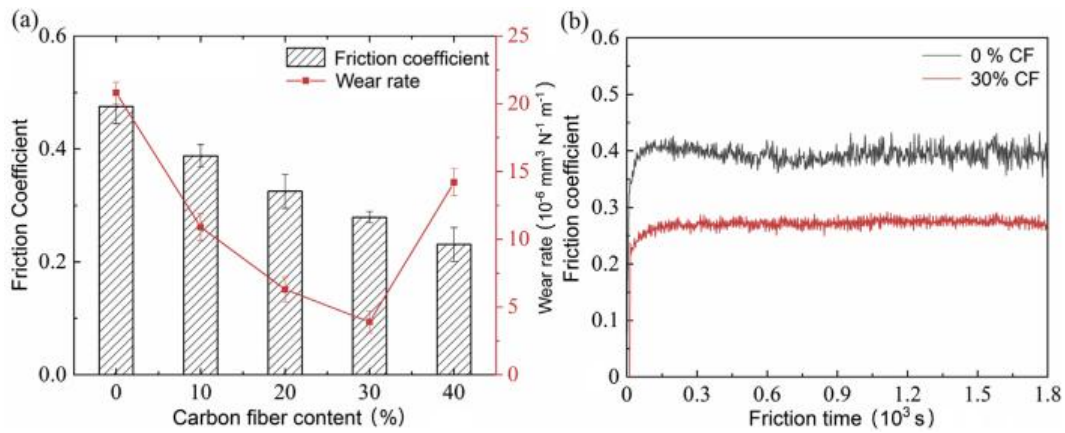
Fig. 7. (a) Fiber content versus COF and specific wear rate, (b) friction coefficient versus friction time.
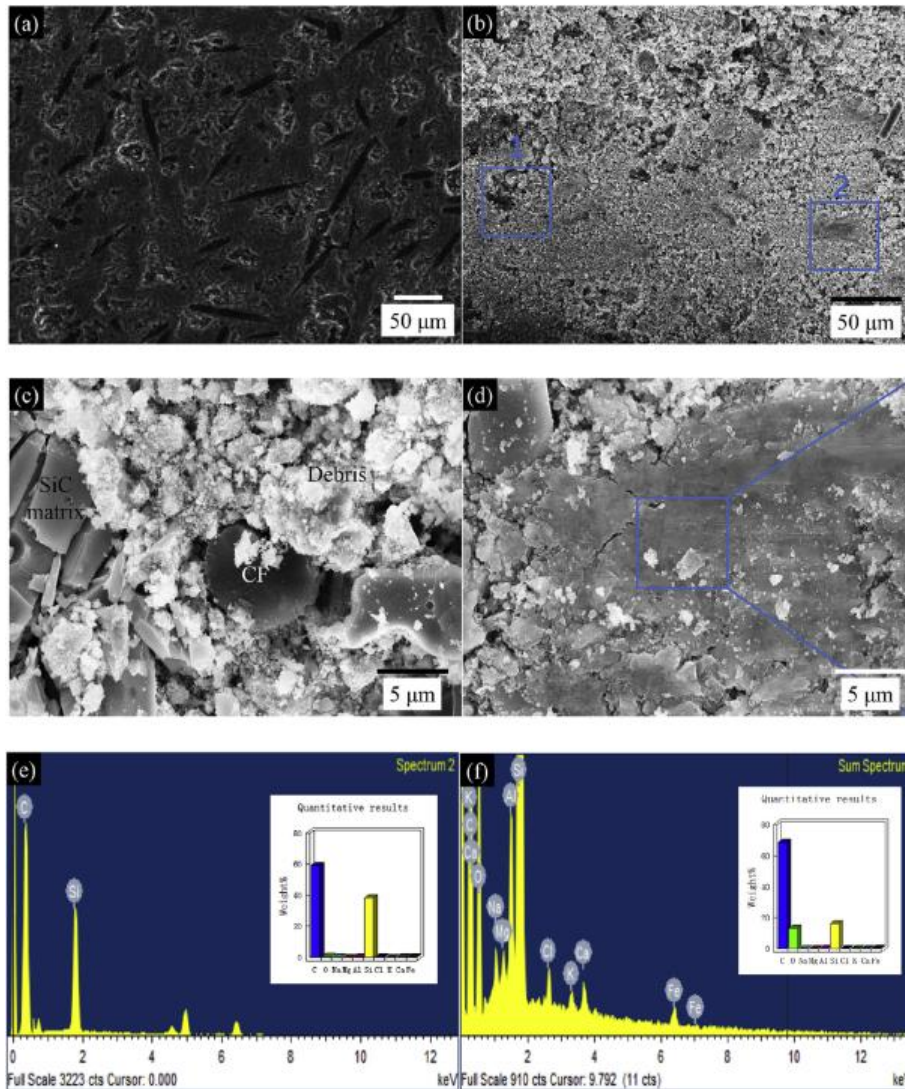
Fig. 8. Wear surfaces before (a) and after (b) testing, (c and d) larger magnifications of the insert areas of b, EDS analysis before (e) and after (f) testing.

size of SiC debris present a significantly higher number of interfaces [42].

As the friction went on, the SiC debris and carbon powders were compacted into continuous friction films on wear surface under high contact pressure, creating protective coatings by decreasing the stress transferred across the wear interface. EDS results in Fig. 8f confirmed

that the O content increased significantly after wear testing, indicating SiC debris was oxidized and SiO_2 films were formed, which were destroyed by the severe mechanical force before transforming into adsorption layer and reactive layer. This repeated friction behavior triggered the adhesive wear mechanism at this stage. Besides, oxidation wear mechanism was also found of great influence on the wear
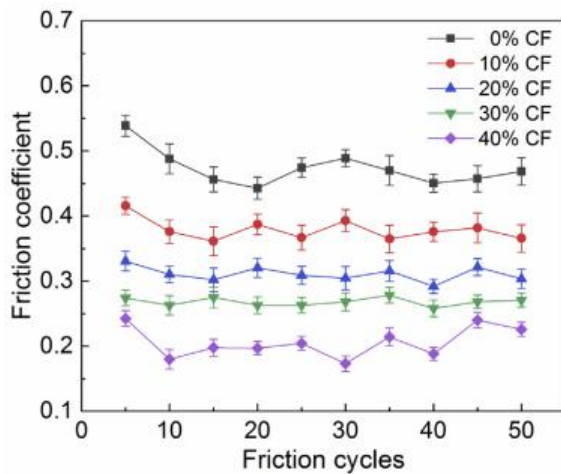
Fig. 9. Cyclic friction performance of C_f/C-SiC composite containing diverse fiber content.

behavior of the composite, due to reaction of the matrix carbon and carbon fibers with the oxygen in the air. The entire chemical equations are as follow [43]:

$$C\ (s) + 1/2\ O_2\ (g) = CO\ (g) \tag{1}$$

$$C\ (s) + O_2\ (g) = CO_2\ (g) \tag{2}$$

$$Si\ (l) + O_2\ (g) = SiO_2\ (g) \tag{3}$$

$$SiC\ (s) + 3/2\ O_2\ (g) = SiO_2\ (l) + CO\ (g) \tag{4}$$

$$SiC\ (s) + 2O_2\ (g) = SiO_2\ (l) + CO_2\ (g) \tag{5}$$

$$SiO_2\ (l) = SiO_2\ (g) \tag{6}$$
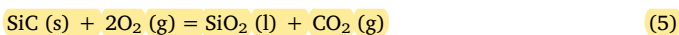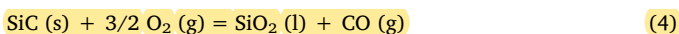
In this work, all samples for wear test were mated with SiC ball for 30 min at a speed of 180 r/min. To facilitate comparison of their cyclic performances, samples were repeated 50 cycles and the results are presented in Fig. 9. Each curve shows a small decline in the beginning, which can be referred to the "run-in" stage of the friction pairs [44,45]. Among various composites, 30% fiber content composite shows the most stable COF due to its uniform microstructural composition. On the contrary, despite of its lowest COF, C_f/C-SiC composites containing 40% fiber content shows severe fluctuations at all stages, indicating fiber agglomeration had happened with excessive fiber content, thus the friction performance became erratic and difficult to predict.

4. Conclusion

C_f/C-SiC composites with diverse fiber content were successfully fabricated by compression molding followed with hot sintering. Microstructures analysis reveals that short carbon fibers are uniformly distributed in C-SiC matrices to form strong bonding and interfaces, providing reliable evidence for the toughening effect of carbon fibers to C_f/C-SiC composite. Mechanical testing reveals that 30 vol% fiber content composite exhibits the highest flexural strength (201.42 MPa) and shear strength (116.68 MPa). Their reinforcing mechanisms can be summarized as fiber pull-outs, fiber debonding and bridging as well as crack deflections. Meanwhile, an improved wear resistance (3.95×10^{-6} mm^3/N·m) and cyclic performances (COF of 0.27 after 50 cycles) was also identified for 30 vol% fiber content composites, due to the combined efforts of abrasive wear, adhesion wear and oxidation wear. These enhanced properties indicating the C_f/C-SiC composites in our work have great potential in braking systems to alternative traditional friction pairs.

References

[1] Krenkel W, Berndt F. C/C-SiC composites for space applications and advanced friction systems. Mater Sci Eng 2005;412:177–81.

[2] Wang HY, Zhu DM, Wan F, Zhou WC, Luo F. Influence of the C/C preform density on tribological characteristics of C/C-SiC composite under different conditions. Ceram Int 2014;40:16641–6.

[3] Tong YG, Bai SX, Hu YL, Liang XB, Ye YC, Qin QH. Laser ablation resistance and mechanism of Si-Zr alloyed melt infiltrated C/C-SiC composite. Ceram Int 2018;44:3692–8.

[4] Fan SW, Sun HD, Ma X, Deng JL, Yang C, Cheng LF, Zhang LT. Microstructure and properties of a new structure-function integrated C/C-SiC brake material. J Alloy Comp 2018;769:239–49.

[5] Krenkel W. C/C-SiC composites for hot structures and advanced friction systems. Ceram Eng Sci Proc 2003;24:583–92.

[6] Cai YZ, Cheng LF, Zhang HJ, Yin XW, Yin HF, Yan GZ. Effects of graphite fillers on the thermophysical properties of 3D C/SiC composites. J Alloy Comp 2019;770:989–94.

[7] Omrani E, Barari B, Moghadam AD, Rohatgi PK, Pillai KM. Mechanical and tribological properties of self-lubricating bio-based carbon fabric epoxy composites made using liquid composite molding. Tribol Int 2015;92:222–32.

[8] Fan SW, Zhang LT, Cheng LF, Tian GL, Yang SJ. Effect of braking pressure and braking speed on the tribological properties of C/SiC aircraft brake materials. Compos Sci Technol 2010;70:959–65.

[9] Pan Y, Iorga L, Pelegri AA. Numerical generation of a random chopped fiber composite RVE and its elastic properties. Compos Sci Technol 2008;68:2792–8.

[10] Paradkar AG, Ravali NS, Prasad NE. Mechanical behavior of 2D and 3D weaved SiC-matrices, carbon-continuous-fibre-reinforced composites: Part 2. Fracture toughness under static loading conditions. Eng Fract Mech 2017;182:52–61.

[11] Xie JB, Liang J, Fang GD, Chen Z. Effect of needling parameters on the effective properties of 3D needled C/C-SiC composites. Compos Sci Technol 2015;117:69–77.

[12] Kumar S, Bablu M, Ranjan A, Manocha LM, Prasad NE. Fabrication of 2D C/C-SiC composites using PIP based hybrid process and investigation of mechanical properties degradation under cyclic heating. Ceram Int 2017;43:3414–23.

[13] Kumar S, Kumari S, Kumar A, Shukla A, Devi GR, Gupta AK. Investigation of effect of siliconization conditions on mechanical properties of 3D-stitched C-SiC composite. Mater Sci Eng 2011;528:1016–22.

[14] Xie JB, Fang GD, Chen Z, Liang J. An anisotropic elastoplastic damage constitutive model for 3D needled C/C-SiC composites. Compos Struct 2017;176:164–77.

[15] Song GM, Li Q, Wen GW, Zhou Y. Mechanical properties of short carbon fiber-reinforced TiC composites produced by hot pressing. J Mater Sci Eng A 2002;326:240–8.

[16] Yang FY, Zhang XH, Han JC, Du SY. Characterization of hot-pressed short carbon fiber reinforced ZrB2/SiC ultra-high temperature ceramic composites. J Alloy Comp 2009;472:395–9.

[17] Liu Q, Huang GQ, Fang CF, Cui CC, Xu XP. Experimental investigations on grinding characteristics and removal mechanisms of 2D-Cf/C-SiC composite base on reinforced fiber orientations. Ceram Int 2017;43:15266–74.

[18] Tang HL, Zeng XR, Xiong XB, Li L, Zhou JZ. Mechanical and tribological properties of short-fiber-reinforced SiC composites. Tribol Int 2009;42:823–7.

[19] Tang C, Dang A, Li TH. Mechanical properties and oxidation resistance of phenolic formaldehyde interlocking CNTs-Cf/SiC composite. Ceram Int 2019;45:9099–105.

[20] Jacob GC, Starbuck JM, Fellers JF, Simunovic S, Boeman RG. Fracture toughness in random-chopped fiber-reinforced composites and their strain rate dependence. J Appl Polym Sci 2010;100:695–701.

[21] Yang FY, Zhang XH, Han JC, Du SY. Processing and mechanical properties of short carbon fibers toughened zirconium diboride-based ceramics. Mater Des 2008;29:1817–20.

[22] Li S, Zhang YM, Han JC, Zhou YF. Random chopped fibers in reaction bonded SiC composite: morphology, etching and reinforcing properties. Mater Sci Eng 2012;551:104–9.

[23] Fan SW, Zhang LT, Cheng LF, Zhang JX, Yang SJ, Liu HY. Wear mechanisms of the C/SiC brake materials. Tribol Int 2011;44:25–8.

[24] Xu YD, Zhang YN, Cheng LF, Zhang LT, Lou JJ, Zhang JZ. Preparation and friction behavior of carbon fiber reinforced silicon carbide matrices composites. Ceram Int 2007;33:439–45.

[25] He XL, Guo YK, Zhou Y, Jia DC. Microstructures of short-carbon-fiber-reinforced SiC composites prepared by hot-pressing. Mater Char 2008;59:1771–5.

[26] Morán MA, Hattum FW, Nunes JP, Alonso AM, Tascóna J, Bernardo CA. A study of the effect of plasma treatment on the interfacial properties of carbon fibre-thermoplastic composites. Carbon 2005;43:1795–9.

[27] Esfehanian M, Guenster J, Heinrich JG, Horvath J, Koch D, Grathwohl G. High-temperature mechanical behavior of carbon-silicide-carbide composites developed by alloyed melt infiltration. J Eur Ceram Soc 2008;28:1267–74.

[28] Yuan H, Wang C, Zhang S. Effect of surface modification on carbon fiber and its reinforced phenolic matrix composite. Appl Surf Sci 2012;259:288–93.

[29] Tikhomirov AS, Sorokina NE, Avdeev VV. Surface modification of carbon fibers

with nitric acid solutions. Inorg Mater 2011;47:609–13.

[30] Woodhead AL, Souza ML, Church JS. An investigation into the surface heterogeneity of nitric acid oxidized carbon fiber. Appl Surf Sci 2017;401:79–88.

[31] Tang C, Li TH, Gao JJ, Kang SL, Xiong CY. Microstructure and mechanical behavior of the Cf/Ti3SiC2-SiC composites fabricated by compression molding and pressureless sintering. Ceram Int 2017;43:16204–9.

[32] Tang C, Li TH, Bai YH, Gao JJ, Yang WB. Two-step method to deposit ZrO2 coating on carbon fiber: preparation, characterization, and performance in SiC composites. Ceram Int 2018;44:11812–9.

[33] Lodhe M, Chawake N, Yadav D, Balasubramanian M. On correlation between β→α transformation and densification mechanism in SiC during spark plasma sintering. Scripta Mater 2016;115:137–40.

[34] Lee E, Lee M, Shim J, Min K, Kim DJ. Microstructure formation of porous silicon carbide ceramics during β→α phase transformation. Int. J. Refract. Met. H. 2017;65:64–8.

[35] Wang W, Fu Q, Tan B. Effect of in-situ grown SiC nanowires on the mechanical properties of HfC-ZrB2-SiC modified C/C composite. J Alloy Comp 2017;726:866–74.

[36] Zhang MY, Li KZ, Shi XH, Tan WL. Effects of SiC interphase on the mechanical and ablation properties of C/C-ZrC-ZrB2-SiC composites prepared by precursor infiltration and pyrolysis. Mater Des 2017;122:322–9.

[37] Zhao Z, Li KZ, Kou G, Liu TY, Li W. Mechanical properties and ablation behavior of C/C-ZrC and C/C-ZrC-SiC composites prepared by precursor infiltration and pyrolysis combined with chemical vapor infiltration. Ceram Int 2018;44:23191–201.

[38] Godfrey D. Friction oscillations with a pin-on-disk tribometer. Tribol Int 1995;28:119–26.

[39] Blau PJ. The significance and use of the friction coefficient. Tribol Int 2001;34:585–91.

[40] Yen BK. Roles of oxygen in lubrication and wear of graphite in "dusting" and ambient conditions. J Mater Sci Lett 1995;14:1481–3.

[41] Li Z, Liu YZ, Zhang BZ, Lu YH, Li Y, Xiao P. Microstructure and tribological characteristics of needled C/C-SiC brake composites fabricated by simultaneous infiltration of molten Si and Cu. Tribol Int 2015;93:220–8.

[42] Fan XM, Xin XW, Cheng Y, Zhang LT, Cheng LF. Microstructure and tribological behaviors of C/C-BN composite fabricated by chemical vapor infiltration. Ceram Int 2012;38:6137–44.

[43] Kim DS, Fischer TE, Gallois B. The effects of oxygen and humidity on friction and wear of diamond-like carbon films. Metall. Coat. Thin Films 1991:537–42.

[44] Cai YZ, Yin XW, Fan SW, Zhang LT, Cheng LF, Wang YG, Yin HF. Effects of particle sizes and contents of ceramic fillers on tribological behaviors of 3D C/C composites. Ceram Int 2014;40:14029–37.

[45] Li Z, Xiao P, Xiong X. Preparation and tribological properties of C fibre reinforced C/SiC dual matrix composites fabrication by liquid silicon infiltration. Solid State Sci 2013;16:6–12.